3 Plane-wave Illumination of Human Phantom

3.1 Introduction

This chapter will first describe how the electromagnetic model of the human phantom and applied plane-wave illumination was constructed to study different phantoms in various scenarios. Two members of the 'Virtual Family' of phantoms were used to represent different human characteristics; gender, height, weight etc. for both occupational and public exposure. There are different exposures limits for public and occupational, due to the exposure circumstances. Detailed information and comparisons are given in the following section of this chapter. The Virtual Family (which was an adjunct to the SEMCAD EM simulation software package) was used extensively to investigate the human whole-body averaged SAR and associated induced current densities. The whole body SAR results from the different phantoms are compared with those published by the UK Health Protection Agency (HPA). Following that, the relationship between the ground plane conditions, human posture and the relationship between human body type and the maximum absorption of electric field is discussed. This includes different ground plane conditions and the techniques used to simulate them.

The previous chapter introduced the numerical methods, commercial software packages and anatomical human phantoms used to simulate human irradiation with plane-waves. SEMCAD and CST microwave studio were used to simulate and compute the reference levels given by ICNIRP. Various parameters of the Virtual Family and modelling techniques were tested. In order to validate the credentials of the phantoms which were used in this research, appropriate parts of the model and results are compared with earlier work carried out by the UK HPA using their own 'Norman' phantom. Furthermore, the significant influence of the 'ground' (conductivity) on the Whole Body Specific Absorption Rate (WBSAR) calculation was noted and explored fully.

This chapter has three main parts:

- Anatomical human voxel phantoms - validation and plane-wave illumination simulation to ICNIRP guidelines.
- Effects of the modelling techniques on the calculations of averaging whole-body specific absorption rate in both homogenous and heterogeneous human phantoms.
- Derived electric field value comparison with ICNIRP reference level and basic restriction comparison and analyses.

A series of investigations into the characteristic electromagnetic fields associated with a high power transmitting antenna were carried out by building an electromagnetic model of the antenna, its infrastructure and ground conditions. These investigations are covered in Chapter 4. Field measurements and comparison of these with the results of simulation will be presented in subsequent chapters.

In the first part the relationship between SAR in the body and plane-wave electric field exposure is investigated. Validation and correlation is also used to assist further human phantom exposure in the third part. Software simulation techniques used in part one to assess compliance with the basic restrictions of ICNIRP for human exposure in a high strength near-field of an HF curtain antenna are also used in stages two and three.

This study uses commercially available high resolution human phantoms – the Virtual Family - and numerical codes – NEC4, CST Microwave studio and SEMCAD. Building on the HPA research (which itself was based on programs written in Fortran in 2006), these software packages are used to examine the problem of human exposure in the complex near field of a real HF curtain antenna. Compared with writing numerical code 'in-house', commercial packages are less time consuming and easily accessed by others who might be interested in such research. These packages also allow a quick application from one to a similar highly complex EM problem, in this case this would be other similar transmission sites. NEC4 was used to model a specific BBC HF antenna and it is associated ground conditions, establishing the EM 'near-field' using the method of moments. Both CST and SEMCAD are compatible with voxel human phantom SAR computations.

3.2   Various human phantoms for plane-wave radiation modelling method

As described in Chapter 2, ICNIRP sets limits for SAR as the basic restrictions as human exposure safety guidelines. These limits are based on an average temperature rise of one degree Celsius in a particular time period. However the actual limits are set at a fraction of the level that would cause this temperature rise. ICNIRP gives restrictions and reference levels in different frequency ranges. Table 2.2 shows the relevant ICNIRP reference levels for signals between 100 kHz to 10 GHz. At 6 MHz the reference levels are 101.7V/m for occupational exposure and 35.5 V/m for public exposure [3.1]

In the relevant literature human phantoms have been subjected to plane-wave radiation in order to study the mechanisms for energy absorption within a human body exposed to EMF [3.2], [3.3]. It is technically impossible to carry out direct measurements of the SAR within a human body. This is particularly true given the complicated nature of the problem under investigation. For this reason numerical modelling and simulation are the principal research methods. This section will elaborate on the human phantoms and modelling methods that have been used such as UK HPA research on MF frequency band antennas emissions [3.4]. The research reported in this thesis continues from that conducted by the HPA and commissioned by BBC World Service, to consider other aspects of human phantom modelling and exposure conditions in relationship with the coupling that exists between an electric field and the human body. The commercial Virtual Family human phantom and HPA Norman models are described briefly along with the research in this area. This will provide a better overview on how solutions for the EM problem are approached. Finally, the whole-body averaged SAR and ankle current calculation results of two phantoms studied will be presented and compared with HPA work and ICNIRP guidelines.

The estimation of radiation absorption for human exposure using very accurate numerical phantom models has been widely used. Because non-invasive measurement of the SAR over the whole human body is difficult, researchers are always looking for alternative accurate and reliable methods for estimating the interactions between electromagnetic fields (EMF) and biological tissues. Human RF exposure health and safety concerns have

attracted a great deal of attentions in many multidisciplinary researches. Only recently have heterogeneous anatomical human phantoms become commercially available for a wide-range of research studies.

3.3　Modelling techniques and effects

Given that 0.4 W/kg [3.5] is insufficient to cause any measurable change of body temperature, it is necessary to investigate this through a credible representative EM model rather than making measurements on real people. The first step is to define a suitable modelling method and human phantom. In this study, the influence of differences such as gender, weight and height on the human body's absorption of energy in a plane-wave electric field are demonstrated. The process is similar to the real diversity of human exposure in EM fields. There are differences between Norman and Virtual Family. The impact of the differences is explored.

Prior to working with a full body voxel human phantom, the FIT based CST microwave studio was tested by modelling and comparing a simplified homogenous human phantom with HPA Norman. The simplified phantom ('Cylinder Man') consisted of a number of cylinders, ellipsoids and cuboids which were based on an average adult male geometry. This first-attempt was to investigate the software potential on SAR calculation. At the time anatomical human phantoms such as the Virtual Family (SEMCAD) [3.6] and 'Hugo' (CST microwave studio) were not commercially available. Cylinder Man also served to investigate the relationship between the incident field polarization and the absorbed energy at various frequencies as well as the relationship between current density distribution and the body cross section.

3.3.1　Homogenous phantom

Two simple homogeneous human phantoms comprising cylinders, ellipsoids and cuboids filled with human body liquid were modelled as shown in Fig. 3.1. The 'standing' and 'arms-out' homogeneous phantoms were built as a preliminary study. Both were illuminated by 1V/m horizontally and vertically polarized plane-waves. For the purpose of this study, a Perfect Matched Layer (PML) was used on the computational boundary box.

This choice of a perfect matching layer (PML) was necessary to avoid spurious reflections at the boundaries of the computational domain. A standing human body tends to be more sensitive to a vertical E-field (Ez) due to the greater electrical length and because of the complementary monopole image of the person in the earth. The standing person with arms stretched out acts as a 'T' monopole which increases the coupling to a horizontal E-field (Ey) as shown in the Fig 3.1. Since there is no complementary image present, the ground effect coupling is less. Additionally, the 'T' monopole has a greater effective electrical height and so is also more sensitive to any vertical field. In the case of a HF broadcast site, the field variations over the dimensions of the human body (such as field variation between 0.2m and 1.7m - which are approximately human ankle and shoulder height - are much larger than at an MF site. These have been studied and will be given in details in following chapters.

Although the EM near-field of HF antennas is non-uniform, the simulations still assume uniform field conditions as a plane-wave irradiation. The assessment considered both the horizontal and the vertical components. The significance of each component is likely to vary from one antenna to another and also with the location within each of the transmitter sites. In some cases the vertically polarized E-field is dominant. In such cases, the currents induced in the leg by the incident external vertical electric field could be a restrictive quantity against the reference values of the ICNIRP guidelines [3.4]; the localized SAR in leg is the most restrictive quantity. In some cases the horizontal polarized E-field component is dominant. In these cases, the wrist current would be the most restrictive quantity due to the better coupling between stretched arms standing posture of human body. In Chapter 4 the studies will focus on the modelling of the primary array. Studying the near field distribution characteristics of an HF antenna helps to identify the most restrictive quantities. The current in the ankle or wrist can be used as measurable quantity for monitoring purposes. This is closely investigated in this study along with SAR [3.5]. This approach makes these estimated safety guideline limits become more accessible. The ankle current measurements can be easily used on site for engineering monitoring.
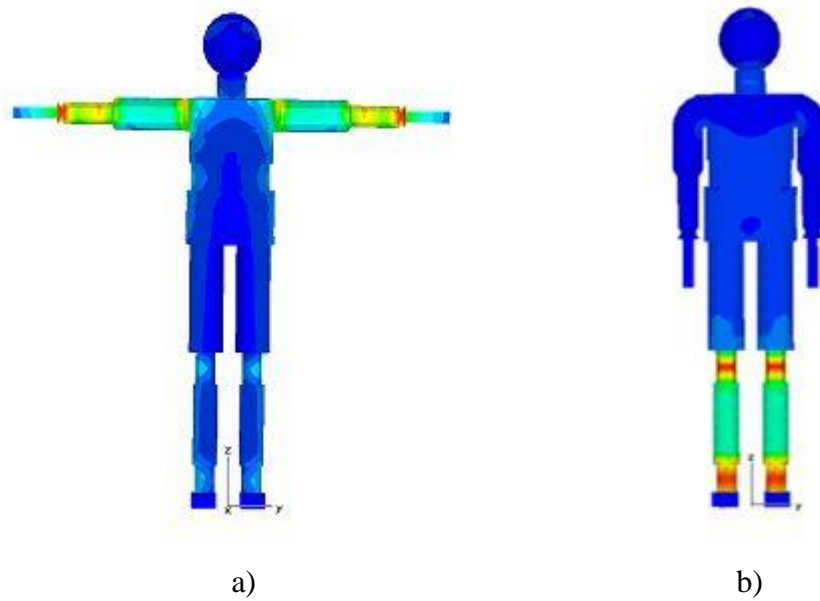
a)   b)

Fig 3. 1 Simple phantom illuminated by (a) horizontally and (b) vertically polarized 1V/m
plane-wave at 6MHz (max->min: red->blue).[3.7]

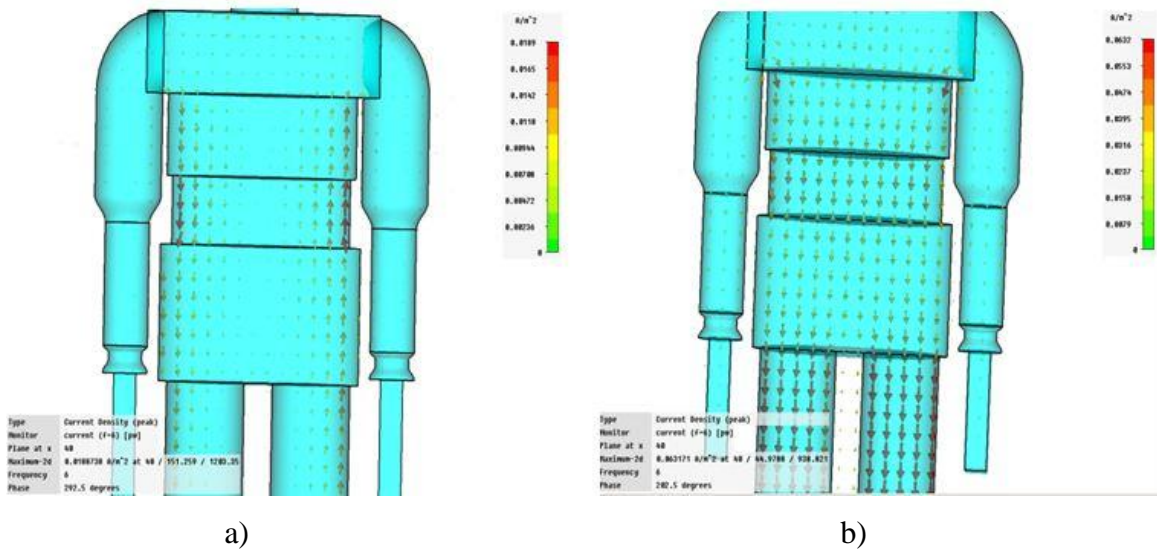a)   b)

Fig 3.2 Current density distribution in homogenous human phantom [3.7]
a) Horizontally Polarized E-field Plane-wave Illumination
b) Vertically Polarized E-field Plane-wave Illumination.

The simple homogeneous phantom was first used to expedite analysis of the effects of changes in basic configuration. Almost 53% of the human body is water. Therefore the material of the homogeneous phantom was water based body tissue simulating liquid with $\varepsilon_r = 59.4$ and $\sigma = 0.84$ S/m. The phantom was either stood barefoot on perfect ground (grounded) or with 2cm thick rubber shoes. The ankle and wrist thickness were 100 mm and 30mm and their radiuses were 40mm and 30mm. The narrowest part of the body is the wrist area with 10mm. Phantoms are arms down by the side or outstretched, and illuminated with either a vertically or horizontal polarized E-field component. Fig. 3.2 shows the current density distributions in the homogenous human phantom under different polarized plane-wave illumination. Table 3.1 summarizes the results of whole-body SAR and compares these with results of Norman from HPA.

Pose	F (MHz)	With shoes						Grounded					
		Av SAR (µW/kg)			HP	Max SAR (µW/kg) HP		Av SAR (µW/kg)			HP	Max SAR (µW/kg) HP	
		HP*	Norman	ΔEz	HP			HP	Norman	ΔEz	HP		
		Ez	Ez	(Norman/HP)	Ey	Ez	Ey	Ez	Ez	(Norman/HP)	Ey	Ez	Ey
Arms down	6	1.43	2.83	+3.0 dB	0.03	19.73	0.30	2.64	4.89	2.7 dB	0.05	32.39	0.48
	8	2.63	4.44	+2.3 dB	0.02	36.13	0.23	4.88	7.76	2.0 dB	0.04	59.82	0.33
	11	5.33	8.54	+2.1 dB	0.03	72.90	0.25	10.02	14.9	1.7 dB	0.03	122.65	0.25
	13	7.87	12.4	+2.0 dB	0.03	107.42	0.29	14.96	21.6	1.6 dB	0.04	182.64	0.30
	16	13.13	18.2	+1.4 dB	0.08	178.30	0.37	25.28	31.5	1.0 dB	0.05	307.56	0.39
	19	20.65	25.6	+0.9 dB	0.09	278.62	0.57	39.95	43.3	0.4 dB	0.10	483.75	0.59
	22	31.06	35.6	+0.6 dB	0.17	415.76	1.00	58.85	56.9	-0.2 dB	0.18	708.30	1.16
Arms out	6	2.41	N/A		0.05	33.05	0.40	4.56	N/A		0.07	53.99	0.54
	8	4.46			0.06	61.12	0.67	8.52			0.07	100.90	0.66
	11	9.16			0.09	125.42	1.15	17.87			0.09	211.06	1.12
	13	13.68			0.11	186.93	1.48	26.97			0.11	317.89	1.45
	16	23.25			0.16	316.38	2.10	46.04			0.16	539.98	2.05
	19	37.21			0.27	503.57	3.26	71.50			0.27	833.41	3.18
	22	55.79			0.49	749.76	5.56	97.09			0.48	1123.19	5.40

Table 3.1 Vertical and horizontal plane-wave incident at 1V/m.

HP*: homogeneous phantom

In table 3.1 the values of SAR are highest for vertical polarized plane-wave on the grounded phantoms with arms outstretched. The SAR values, with arms outstretched, also increase with frequency, and are ~20dB higher than those for horizontal polarized plane-wave. For vertical polarized field the grounded phantoms have SAR's that are approximately twice those of phantoms with shoes, and the SAR's of phantoms with arms outstretched similarly exceed those with arms down. However with horizontal polarized plane-wave the effect of the shoes is not as pronounced. Generally a grounded phantom has the strongest coupling to a vertically polarized plane-wave, compared with wearing shoes or being isolated with no ground present as shown in Fig 3.1. This is due to the complementary monopole image in the earth increasing the electrical length and so helping resonance. In addition, a phantom with outstretched arms forming a 'T' monopole has stronger coupling to a horizontally polarized plane-wave than with arms by the side, due to the increased co-polar current path in the former case, but this coupling is still less than with the vertically excited grounded monopole due to the shorter co-polar element. Thus incident field levels required to produce restrictive SAR's are generally significantly higher for horizontal polarization. In HPA studies, the Norman model was only considered grounded with and without shoes with Ez irradiation. Comparing the whole-body SAR of Norman with the Homogenous phantom (see Table 3.1), Norman shown higher SAR in all simulations excepted when grounded without shoes at 22MHz. The homogenous phantom was 'filled' with water based, body tissue simulating liquid, which is similar to the human natural body consistency. However, in a real person, the ankle and wrist region have high conductivity muscles but also have the narrowest cross section of any part of the human body. In this case, the localized SAR calculation would require a more refined voxel phantom rather than simple homogenous phantom as seen in Fig 3.1. For more accurate RF radiation hazard assessments, realistic human phantoms were explored further in this chapter.

3.3.2   Heterogeneous phantom

Duke, the adult male from the Virtual Family was used in the initial investigation. Fig.3.3 is a centre vertical cut 2-D SAR distribution obtained when Duke was irradiated by a plane-wave. Fig.3.4 is a cross section of Duke's ankle and wrist area. In all simulations the

phantom is located on a pre-defined ground plane and is surrounded by a region of air. A 3D mesh is defined according to the model voxel resolutions. The air region surrounding the phantom is connected to be a perfectly matched layer (PML) [3.8] as a boundary condition to reduce the reflected scattered field. This is to diminish interference and minimise the simulation errors [3.6]. A further investigation on the PML variations effects on the model was also carried out and presented in the following section of this chapter.
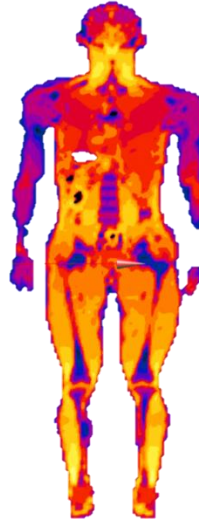

Fig. 3.3 Duke SAR distribution.

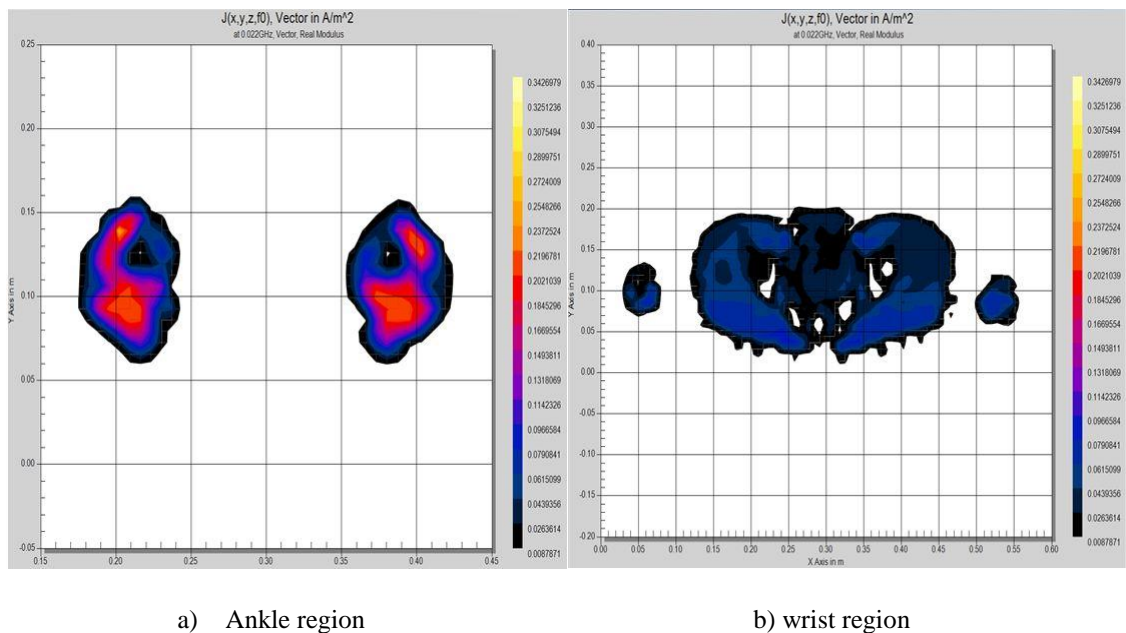a)   Ankle region   b) wrist region

Fig 3.4 Current density distribution of Duke Phantom in SEMCAD.

Table 3.2 shows comparisons between the high resolution HPA Norman and SEMCAD Duke phantom with arms down, illuminated by a 1V/m vertically polarized plane-wave and isolated in space. Agreement between the two phantoms is quite good, bearing in mind that Duke has approximately double the number of tissue types. Unfortunately, due to limitations of the software, the Virtual Family phantom could not be altered its posture for wrist current calculation.

Quantity	Norman[3.1]		Duke	
	6MHz	22MHz	6MHz	22MHz
Ankle current (mA)	0.195	0.648	0.166	0.643
Wrist current (mA)	0.010	0.062	0.010	0.081
SAR (μW/Kg)	0.536	6.99	0.564	7.56

Table 3.2 Comparison between Norman and Duke Phantoms for 1V/m vertical plane-wave incident at 6 MHz and 22 MHz isolated.

3.3.3   Perfect matching layers

Perfectly matched layer (PML) boundary conditions [3.9] are used to reduce the E-field reflections into the computational domain. Fig. 3.5 shows a cutaway view of the computational domain enclosing the PML, free space and voxel phantom. The width of the free space region is denoted "a", whist the width of the PML layer and distance from the interface are denoted by the letters "b" and "ρ" respectively [3.10].
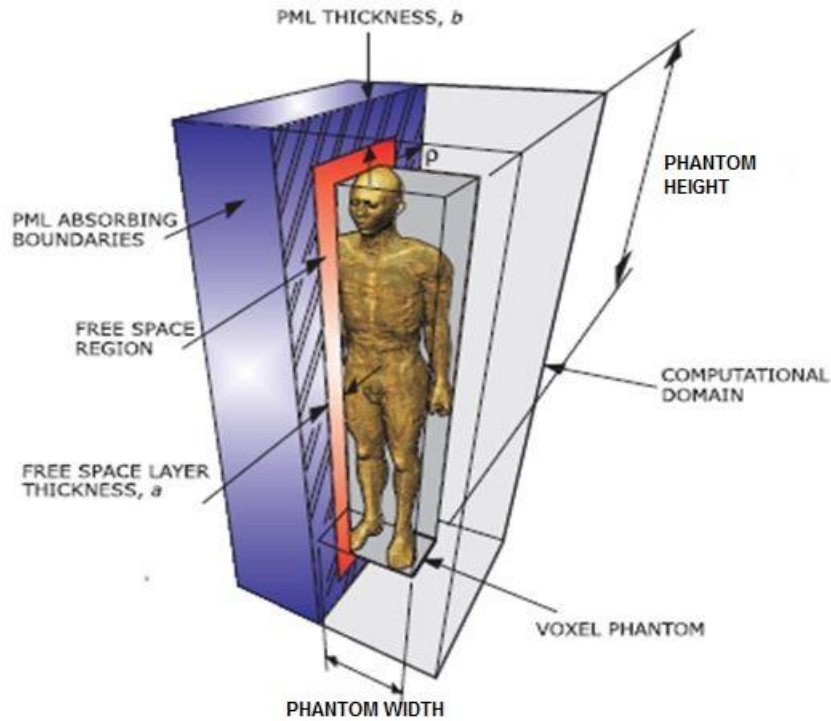
Fig 3.5 Variations in calculated SAR with distance to the perfectly matched layer
boundary for a human voxel model [3.10].

As frequency increases, smaller cell sizes are required so that an adequate sampling of the
waveform can be performed. When the voxel is in the arms-out pose the volume of the
computational domain is almost doubled. The virtual family models and the posed models
already use quite a lot of computer RAM; this is then shared with the RAM needed to
extract the SAR. For whole-body SAR calculations, the time step is related to the
resolution of the model. The computational effort required is proportional to the reciprocal
of the forth power of the cell size [3.11].

Voxel size	Computation time	Pml layers
2mm	>24 hrs	2 cell
4mm	≈9 hrs	6 cell
6mm	≈4 hrs	6 cell

Table 3.3 Voxel resolution size, PML layers and computational time.

A set of models were simulated using different PML layer settings in SEMCAD. The
results indicate that increasing the number of PML layers did not cause any changes in the
results. However this reduced the computational time required as shown in Table 3.3. The

results therefore support the continued use of a 2-cell free-space layer together with a 6 cell wide PML in the FDTD code. It is also important to use split-field PML based boundary conditions, as first advocated in the studies by P. J Dimbylow [3.10]. A Huygen Surface [3.12] was implemented in the FDTD code to allow the description of arbitrary fields. In this way it is possible to separate the scattered fields (that are required for the boundary conditions) from the total field required for the FDTD formulation. It also enables a connection to be formed between the PML layers and the inner region of the computational domain [3.13] which also used for further hybrid methods studies of this thesis as discussed in previous section.

3.4 Equivalent principle and FDTD hybrid methods for whole-body SAR calculation

The Equivalent principle (as introduced in chapter 2) and FDTD hybrid methods would allow the phantom to be illuminated in a non-plane-wave environment. A reactive near field with elliptic polarization could significantly affect the relationship between incident field level and induced SAR. For this reason it was necessary to modify the conventional method of assessment, based on a plane-wave incident on the whole body. Also the modelling strategy employed by the HPA involved using Scalar-Potential Finite-Differences (SPFD) = limb SAR/induced current, and FDTD = limb current / incident field. These can be modified to use MoM-FDTD hybrid as investigated in this study. The HPA used quasi-static SPFD to increase efficiency for higher resolution. Here FDTD is used to calculate SAR directly [3.7]. The hybrid method is adopted to combine both Equivalent Principle and FDTD methods together. This method is based on two computational techniques, the Method of Moments (MoM) [3.14] and FDTD algorithms[3.15], implemented by software packages NEC4 [3.16] and SEMCAD-X [3.17] respectively. The MoM technique is best suited to computing scattering from conducting wires and surfaces, whilst FDTD is more appropriate for the analysis of volumetric dielectric bodies. This makes it possible to analysis human exposure in the complicated scenario in the near-field zone of a real HF antenna standing on real ground. Compare with FDTD, MoM requires much less computing time and hardware resources which could, potentially, significantly increase the efficiency of SAR calculation. In this case the

Total Field Scattered Field (TFST) algorithm (Equivalent Principle) [3.12] is used to link MoM and FDTD together. A TFSF based 'Huygen Box' would be used to import the HF array calculated near field using NEC4 into SEMCAD. With the Huygen Box surrounding the phantom, incident plus phantom-scattered fields are then computed within this box, for SAR calculation. Before a complicated antenna near-field values as the Hugen Box excitation, a plane-wave was used instead to test this method.

Table 3.4 compares limb currents and whole body averaged SAR values calculated by the HPA with those calculated using SEMCAD, The results obtained by the HPA apply to the Norman phantom, whilst those obtained with SEMCAD apply to the Duke phantom and were calculated. It shows ankle current (mA), wrist current (mA) and whole body average SAR (μW/kg). These were calculated for different voxel sizes and for both vertical plane-wave illumination of the phantom at 1V/m (rms), and using Huygen Box.

Phantom	Excitation	Voxel size (mm)	6 (MHz)			22 (MHz)		
			Ankle (mA)	Wrist (mA)	SAR (μW/Kg)	Ankle (mA)	Wrist (mA)	SAR (μW/Kg)
Norman	PW	2	0.195	0.010	0.536	0.648	0.062	6.990
Duke	PW	4	0.166	0.010	0.564	0.643	0.081	7.560
			(0.85)	(1.00)	(1.05)	(0.99)	(1.31)	(1.08)
		6	0.169	0.010	0.615	0.626	0.078	7.290
			(0.86)	(1.00)	(1.15)	(0.97)	(1.26)	(1.04)
	PW + HB	4	0.143	0.010	0.515	0.579	0.085	7.100
			(0.73)	(1.00)	(0.96)	(0.89)	(1.37)	(1.02)
		6	0.146	0.009	0.541	0.575	0.082	6.810
			(0.75)	(1.00)	(1.01)	(0.89)	(1.32)	(0.97)
	HB	4	0.162	0.010	0.541	0.614	0.092	6.580
			(0.83)	(1.00)	(1.01)	(0.95)	(1.48)	(0.94)
		6	0.565	0.565	0.565	0.614	0.095	6.280
			(1.05)	(1.05)	(1.05)	(0.95)	(1.53)	(0.90)

Table 3.4 Comparison between Norman and Duke phantoms for 1V/m vertical plane-wave incident at 6MHz and 22MHz.

PW: Plane-wave excitation;
PW+HB: Plane-wave excitation with Huygen Box implemented in SEMCAD (as HPA);
HB: Huygen Box import with external plane-wave field values.
Duke/Norman agreement ratio in (bold).

The simulation results are shown to be in good agreement with the UK HPA results. The agreement ratios between the calculated results and those from the UK HPA are shown in (bold) in the table 3.5 [3.18]. The Whole body SAR values are of special importance as they are one of the basic references in ICNIRP guidelines. It should be noted that there are differences between the Duke and Norman phantoms in terms of height, weight, number of tissue types and voxel resolution in the simulations and so some degree of variation in the agreement ratios can be expected. The Huygen Box plane-wave excitation is also in a good agreement to the results produced by the UK HPA. However, the interface between NEC4 and SEMCAD was limited by the development of the Software. When considering application of a full scaled antenna EMF field import, further validation is needed.

3.5   Whole-body SAR calculations

Studies of various conditions are presented; shoes, tissues, gender, ground coupling. Several aspects of these conditions are considered.

Understanding how various ground conditions affect the induced current density within a human body is essential for accurately predicting the basic occupational exposure restrictions in the near-field of a high power HF transmitting antenna. This part of the study provides a comparison with that performed by the UK-HPA and extends it further. These scenarios of ground conditions for an average adult male are: barefoot touching the ground; with shoes; and isolated from the ground (in free-space). In the UK-HPA's work [3.1], [3.19], the ground was considered to be a perfectly conducting ground plane. Although the barefoot and perfect conducting ground scenarios are unrealistic, they enable comparison of the numerical method used to calculate whole-body SAR.
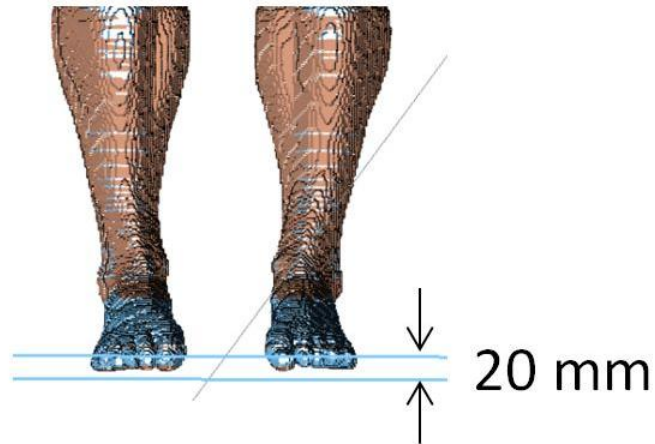
Fig 3.6 2 mm voxel resolution of human phantom's feet (Duke).

For comparison with the results from the UK HPA, the human phantom (Duke) was illuminated by a 1 V/m (rms) vertically and horizontally polarized plane-wave at 6MHz in both CST Microwave Studio and SEMCAD. Both models are arms down beside the bodies. The UK-HPA model considered Norman with a 20 mm thick rubber shoes layer or, barefoot standing on a perfect conducting ground plane, as shown in Fig. 3.6. It was also applied in this chapter for comparison purpose. In addition to shoes, the variations of the ground conditions are considered along with its effects on whole body SAR results. These results are compared with UK HPA Norman results below (Table 3.5).

	Duke		Norman	
	WBSAR (µW/kg)		WBSAR (µW/kg)	
	Ez	Ey	Ez	Ey
Isolated	0.374	0.09	0.536	0.113**
WS on a PEC brick+	4.64	0.158	2.83*	N/A
WS on a PEC boundary ***	1.393	0.125		
WS on AVG+	2.29	0.068	N/A	N/A
BF on PEC brick	5.56	0.175	4.89*	N/A
BF on PEC boundary ***	0.677	0.122		
BF on AVG	2.22	0.0693	N/A	N/A

Table 3.5 Whole body SAR of Duke (arms down) when illuminated by 1W vertical (Ez) and (Ey) polarized plane-wave for various ground conditions in CST.

*HPA report states Norman with shoes and barefoot on a perfectly conducting ground plane but the PEC conditions are undefined.
**HPA only modelled Norman illuminated by horizontally polarized plane-wave (Ey) isolated in space for the arms down scenario.
*** CST default boundary condition
+Both PEC brick and average ground here are 1 m thick
BF: barefoot standing
WS: with shoes layer
AVG: average condition ground

Realistic average ground has been represented as a 'lossy' brick with dielectric properties of $\varepsilon_r = 13$ and $\sigma = 0.005$ S/m, below which a CST default PEC boundary condition has been used. Perfect Electric Conducting (PEC) grounds have been modelled using both the CST default PEC boundary condition and as a solid brick. A 2 cm thick rubber layer ($\varepsilon_r = 3.2$ and $\sigma = 0$ S/m) was used to model shoes, placed between the bottom of the bare foot and the ground. A PEC condition was placed underneath the ground brick to minimize the reflection of the scattered field, so it can be seen as an infinite ground to calculate to SAR. The different thicknesses of ground bricks were modelled to examine, the effects of ground brick thickness on SAR. The values and variations are presented in the following section. Results were compared in Table 3.5. For all scenarios considered, the vertical component of the E-Field (Ez) is much greater than the horizontal (Ey) component.

It can be seen in Table 3.5 that the WBSAR values obtained through simulation in CST microwave studio are not the same as those obtained by the HPA for the Norman phantom. The scenario of isolated, with shoes on a 1m thick ground plane, barefoot on PEC brick differs by about 20%. Also, it can be seen that in general, if the ground condition is

represented by a brick whose dielectric properties match those of the average earth, Duke has higher WBSAR values. The WBSAR of Duke appears to be about 30% lower with vertical plane-wave illumination and 20% lower when the E-field component is horizontal and the phantom is grounded by the software default PEC boundary condition. In the CST microwave studio models, the results obtained for Duke do not seem to be influenced by presence of the shoes when standing on an average ground brick but quite the opposite is true when the PEC is used as the boundary condition. It is interesting to see that the ground condition of the computational software had such significant effects on WBSAR.

3.5.1 Phantom complexity

This part of chapter addresses the complexity of the phantom and the effects on whole body SAR values, including the number of tissue types and the voxel resolution. The effects of gender and body size of different phantom resolutions are considered as well.
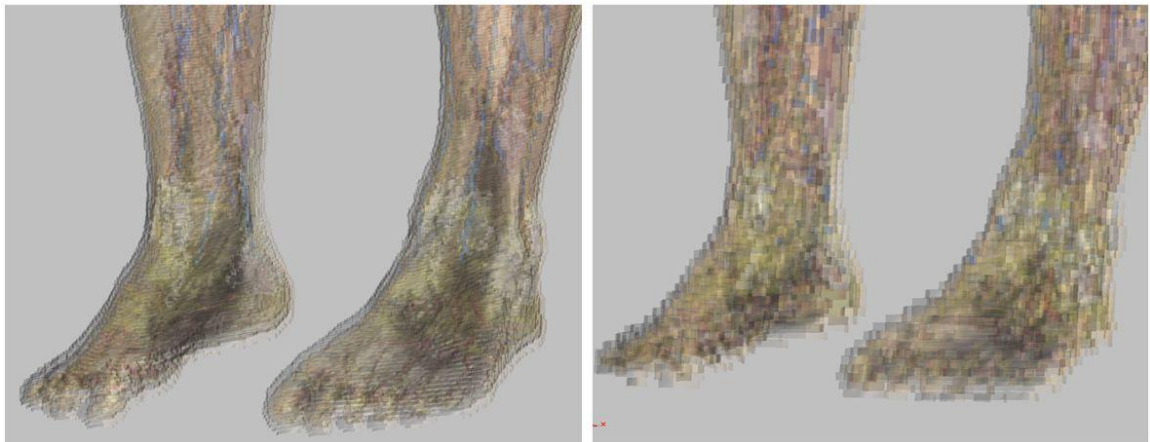
a) 2mm   b) 4mm

Fig 3.7 voxel size resolution variation.

Each voxel of an anatomical human phantom defines the mixture of the different materials that compose it. Voxelized phantoms are widely utilized in modeling of the human body for computations of medical phenomena, exposure to ionizing radiation and other environmental stimulations. SEMCAD has a built in Graphic User Interface (GUI) that allows the user to re-scale the voxel size of the human phantom. Increasing the resolution could increase the accuracy of computation results, it can be very useful when considering more sensitive high risk regions of human body such as localized SAR in the brain, heart

etc. These would mainly be of interest for lower power-frequency fields (extremely low frequency electromagnetic fields; ELF) and from radiofrequency/microwave radiation emissions (RF) from wireless communications. Fig 3.7 compares a 2mm voxel phantom with 4mm voxel phantom. Considering the 2mm resolution model, Duke's feet appear clearly smoother and there is more anatomical detail. The significant advantage of such high resolution is that it provides a closer match to the real human geometry, as well as more tissue and organ types. When increasing the frequency, the volume meshing technique requires a smaller cell size to ensure adequate sampling of the waveform, which means a longer computing time. However, increasing the voxel size will cause a voxelized human to have too many voxels (near the surface of the body) which contain both body tissue and external air. The 'captured' air will lead to inaccurate results. For this reason adequate resolution of the human phantom is required. By studying the relationship between the voxel size and number of tissue types from the WBSAR simulation results and by comparison with HPA and ICNIRP guidelines the aim is to help find appropriate parameters when apply the method in to a range of this similar EM problems.

Table 3.6 compares both Duke and Norman's WBSAR results when subjected to plane-wave irradiation in CST microwave studio. In these simulations the human phantom is located 2 voxel cells (4mm) from the boundary. A free space layer of 2 cells is the minimum boundary spacing requirement for FDTD calculation [3.11], [3.10]. Enlarged spacing will increase the meshing resolution and computation difficulties; 6 layers of PML is adequate for the calculations [3.10]. The results of Table 3.6 were re-plotting in Fig 3.8 with error bar shows about 10-15% variations.

Frequency 6MHz	Duke 32 Tissue type				Duke 77 Tissue Type			
WBSAR (µW/kg)	2mm		4mm		2mm		4mm	
E-field Polarization	Ez	Ey	Ez	Ey	Ez	Ey	Ez	Ey
Isolated	0.381	0.09	0.374	0.09	0.423	0.415	0.391	0.350
BF on PEC brick*	5.43	0.159	5.56	0.175	6.10	0.211	6.73	0.204
BF on a PEC boundary**	0.685	0.127	0.677	0.122	0.724	0.597	0.723	0.607
BF on AVG	1.98	0.069	2.22	0.0693	2.120	0.064	1.989	0.064
WS on PEC brick	3.75	0.178	4.64	0.158	4.237	0.182	4.210	N/A
WS on PEC boundary **	1.20	0.130	1.393	0.125	1.479	0.110	1.284	N/A
WS on AVG	1.93	0.068	2.29	0.068	2.237	0.064	2.106	N/A

Table 3. 6 Whole-body SAR variation of human phantom tissues numbers in CST simulations.

*Both PEC brick and average ground here are 1 m thick
**CST default boundary condition
BF: barefoot standing
WS: with shoes layer
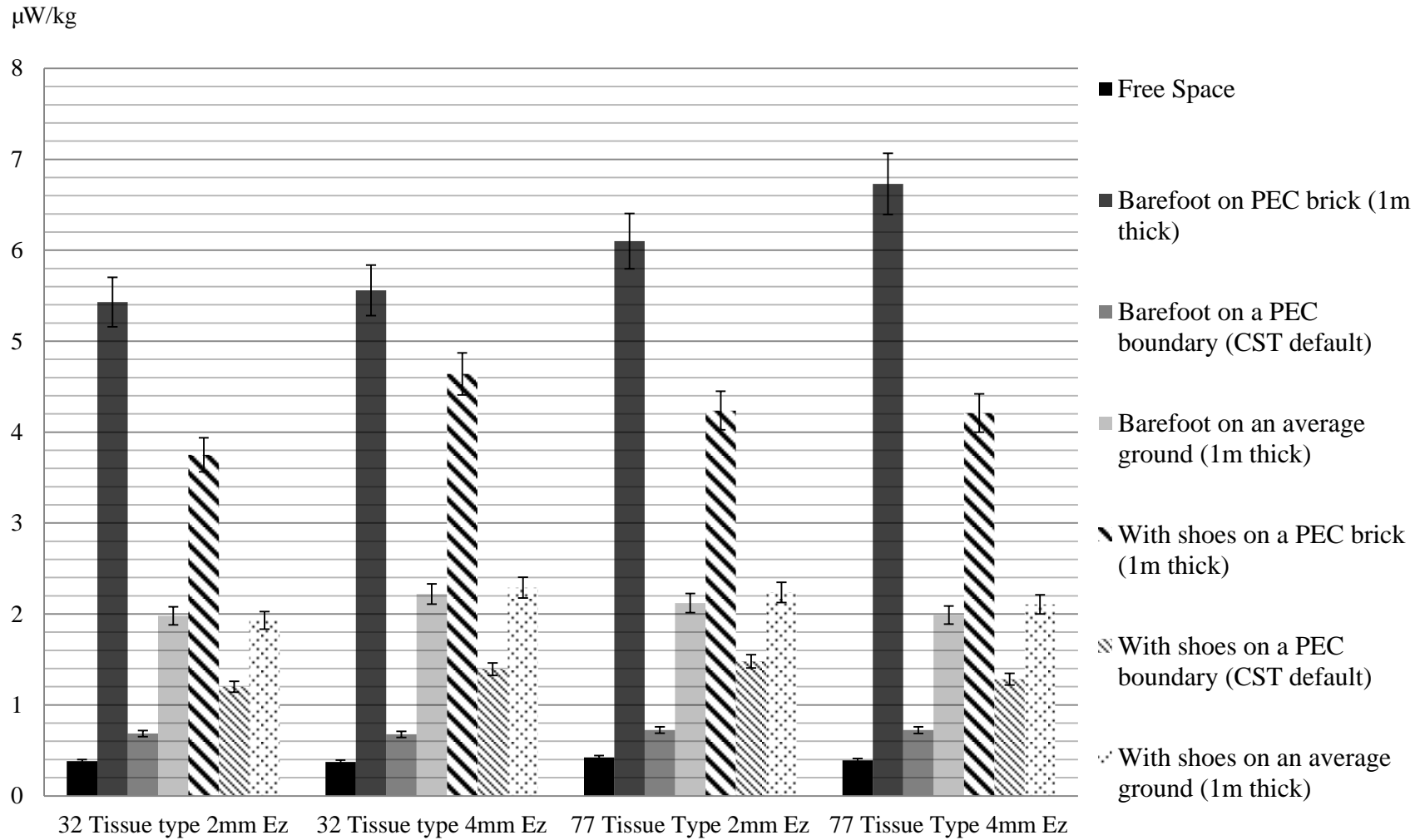AVG: average condition ground

Fig 3.8 Tissue layers variation WBSAR results of various ground condition in CST.

As with most other 3D EM simulation software, CST microwave studio does not allow the dielectric properties for the boundary and the plane-wave irradiation range to be specified. This means that a different approach is required when considering the coupling between a realistic ground and a human. However, when other objects are used to represent the ground conditions; CST microwave studio sees the objects as part of the model rather than a ground conditions. The human would not be seen as standing on an infinite ground plane by the software. In order to keep good consistency when comparing Duke and Norman, 20mm thick rubber layers were also used as shoes in simulations. However this left a small gap between the feet and ground for Duke modelling. For this reason the feet would not be properly grounded when the human phantom was in the standing position. The HPA developed a model using the Norman phantom, where the feet were modified to be totally flat leading to a better calculation of the ground coupling effect. The differences in the 'gap' and ground modelling conditions will cause the results to be different and possibly introduce errors in the whole body averaged SAR (WBSAR) calculation. This indicates that coupling with the ground is an influential aspect of assessing human RF exposure in complex and realistic environments. This is further investigated later in this chapter and will be elaborated further in the next chapter

As mentioned earlier in this Chapter the human phantoms also have physical differences that need to be considered. The Norman phantom contains 32 tissue types, and HPA used 4mm resolution model in the HF frequency band [3.11], [3.1]. In addition to 32 types of tissue, in this study, the Duke phantom with 77 tissue types was considered with the plane-wave illumination using SEMCAD. As with CST microwave studio, SEMCAD could not allocate dielectric properties to specific boundary to represent average ground. However, unlike CST microwave studio, the plane-wave illuminate region is more flexible. This allows implementation of brick to represent a realistic lossy ground into the simulation. The calculated results in SEMCAD of these simulations are shown in Table 3.7. The 'Billie' phantom was also investigated here following the same modelling protocol (Table 3.7). Considering the size of Billie it could be used to represent a female with average height and weight.

Table 3.9 shows the results using phantoms with 77 tissue types and 2mm and 4mm voxel resolution illuminated with a vertically polarized 1V/m plane-wave. The calculated WBSAR results for Duke and Billie are compared and shown in bold red for the 2mm voxels and bold blue for the 4mm voxels.

Some of the results of Table 3.7 are also plotted in Fig 3.9 and Fig 3.10. The error bar shows about 10-15% variation.

Tissue types		Billie 32		Billie 32	Billie 77		Billie 77	Duke 32		Duke 77	
Frequency 6MHz		2mm		4mm	2mm		4mm	2mm	4mm	2mm	4mm
WBSAR (μW/kg)		Ez	Ey	Ez	Ez	Ey	Ez	Ez	Ez	Ez	Ez
FS		0.371	0.060	0.32	0.575	0.072	0.583	0.552	0.560	0.568 (-1%)	0.575 (-1%)
Barefoot	BF on PEC brick*	2.023	0.053	2.49	2.541	0.057	2.314	5.10	4.982	5.166 (+51%)	5.541 +58%
	BF on a PEC boundary**	0.890	0.017	0.90	0.918	0.0194	0.90	1.481	1.618	1.434 (+36%)	0.918 (+2%)
	BF on an AVG	0.993	0.01	0.87	1.093	0.0141	1.10	1.873	1.910	1.925 (+43%)	1.093 (-1%)
With Shoes	WS on PEC brick	0.910	0.013	0.875	0.919	0.015	1.015	2.494	2.31	2.529 (+63%)	0.919 (-1%)
	WS on PEC boundary	0.937	0.010	0.88	0.948	0.009	0.867	1.099	1.28	1.114 (+15%)	0.948 (+1%)
	WS on AVG	0.761	0.006	0.690	0.787	0.007	0.653	1.130	1.21	1.163 (+33%)	0.787 (+17%)

Table 3.7 Whole-body SAR variation of human phantom tissues numbers in SEMCAD simulations.

*Both PEC brick and average ground here are 1 m thick
**SEMCAD default boundary condition
BF: barefoot standing
WS: with shoes layer AVG: average condition ground
77 tissue types and 2mm phantom voxel resolution, variation of Duke results compare with Billie **(Bold Red)**
77 tissue types and 4mm phantom voxel resolution, variation of Duke results compare with Billie **(Bold Blue)**
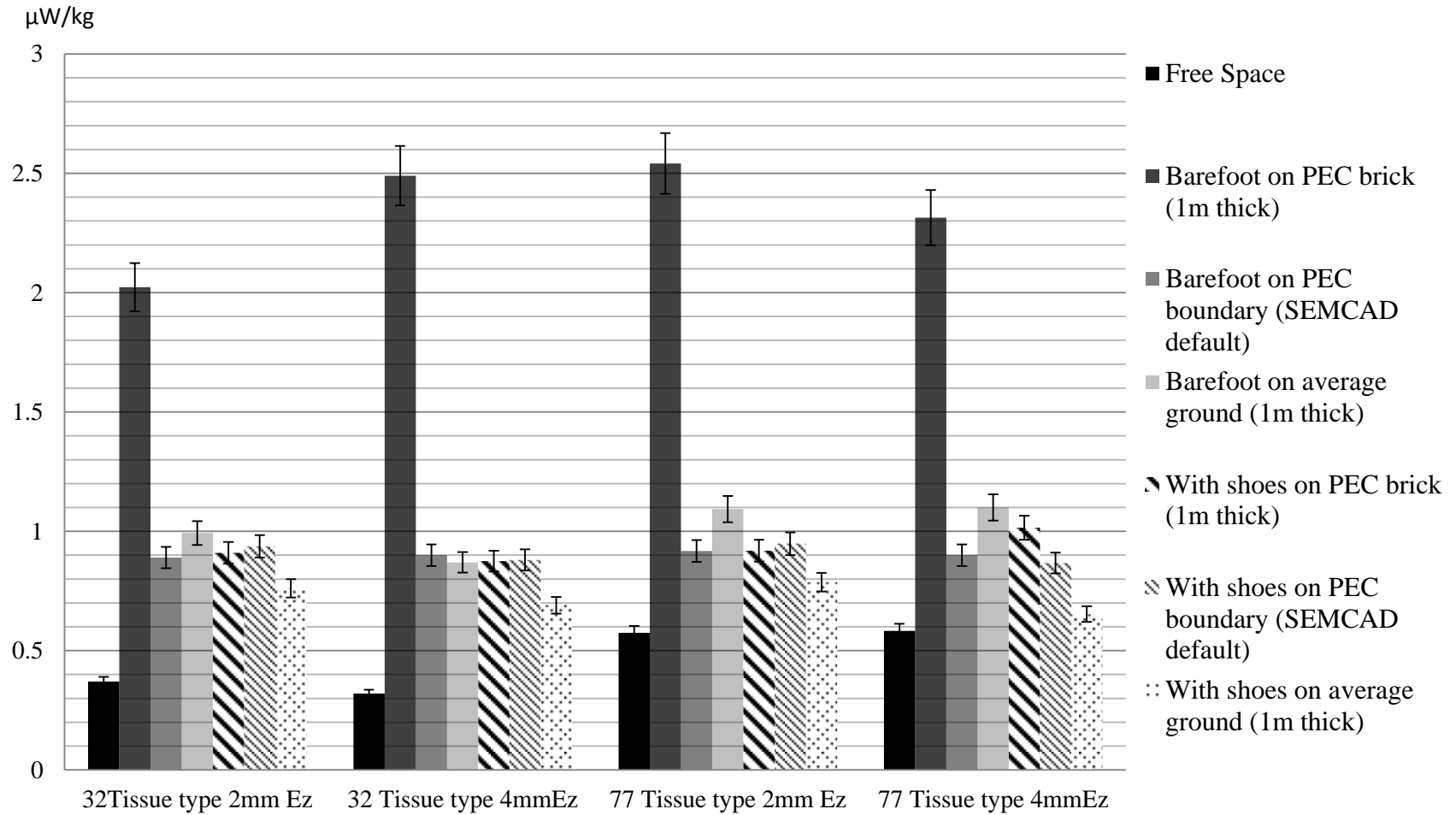
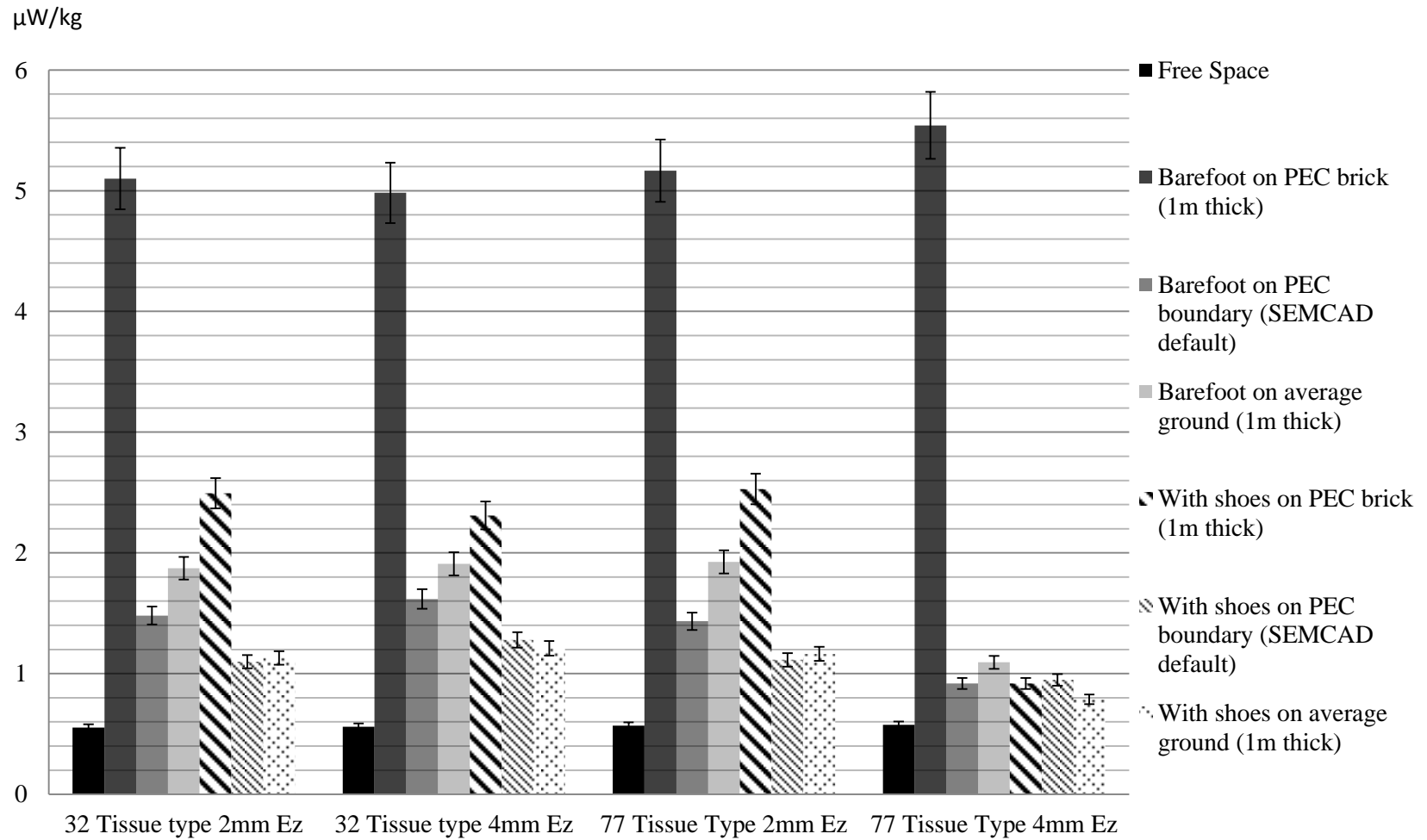Fig. 3.9 Billie Tissue layers variation WBSAR results of various ground in SEMCAD.

μW/kg

Fig. 3.10 Duke Tissue layers variation WBSAR results of various ground in SEMCAD.

Looking at the calculated WBSAR of the Billie phantom with 32 tissue types, the difference between the 4mm and 2mm results is about -1.6% when is isolated. When tissue numbers increase to 77 the difference between the 4mm and 2mm results is about +1.3%. The calculated WBSAR of the Duke phantom with 32 tissue types shows a difference between the 4mm and 2mm results of about +1.4% and when tissue numbers increase to 77 the difference is about +1.5%. For Billie when barefoot standing on a PEC brick, the WBSAR results show the highest variation when voxel size is reduced from 2mm to 4mm in 32 (+23%) and 77 tissues numbers (-9%). Under the same conditions the WBSAR results for Duke show less variation; the difference between the 4mm and 2mm results using 32 tissue types is -5% and using 77 tissue types is +9%. In general the indicated WBSAR using 4mm voxels is smaller than with 2mm voxels. Using 2mm resolution, 77 tissue types and a vertically polarized plane-wave (incident radiation) over various ground conditions; the highest WBSAR for both Billie and Duke appears when the phantoms are barefoot standing on a PEC brick. The lowest values occur when they are isolated.

The number of organs and tissue types within the Duke and Billie phantoms are almost double the number found in Norman. The 'fine resolution', 2mm voxel size phantom is an anatomically realistic voxel model of a human body. When conductivity is averaged, high conductivity appears decrease when the voxel size decrease (resolution increase). This is called conductivity masking[3.20]. The SAR by definition is a function of the induced current. The WBSAR is the total energy absorbed by human body divided by the full body mass. Therefore when the human phantom resolution increases (voxel size decrease), theoretically the WBSAR would decrease as the average conductivity (and hence the current flowing in the tissue) decreases. Both Duke and Billie agree well with this trend using different ground conditions (see Fig 3.9 and Fig 3.10). Coarser resolution would also make it harder to differentiate the tissues in the body. The FDTD (SEMCAD) or FIT (CST microwave studio) discretization process (meshing) before the whole-body SAR calculation limits some certain fine areas of the phantom. The meshing configurations can attribute to certain results variation.

3.5.2　Effects of ground coupling

This section addresses the SAR values obtained as variations in the ground coupling are modelled. The effects of gender/body factor were also considered. When a person stands above a ground plane, an equivalent short circuit current to ground is induced which depends, predominantly, on the square of a person's height [3.21]. Fig.3.11 shows how the simulated whole body SAR in Duke varies for different thicknesses of an average ground ($\varepsilon_r = 13$ and $\sigma = 0.005$ S/m) when illuminated by a 1W vertically polarized plane-wave. In reality the human can be considered to be standing on an infinite ground plane, in a complex EM environment such as an HF broadcasting transmitter site. Both barefoot and with shoes are considered, while a SEMCAD default PEC boundary condition has been implemented below the average ground brick. Using a dielectric brick with certain length to represent infinite ground also need to be validated. Therefore various brick thicknesses were considered. The results of SAR in various ground conditions and thickness were compared with P.J Dimbylow HPA reports. The thickness of the ground brick is varied between 0.5m and 4.5m with 0.5m increments. The thickest brick would be about tenth of the wave length when the frequency is 6MHz. It can be seen that the calculated SAR is highest in the ankles and varies depending on how the ground coupling model is implemented. The SAR distributions within the human phantom, Duke, are shown in the Fig.3.11. As mentioned before, in the vertical polarized plane-wave irradiation case, the highest SAR value would occur in ankle area.
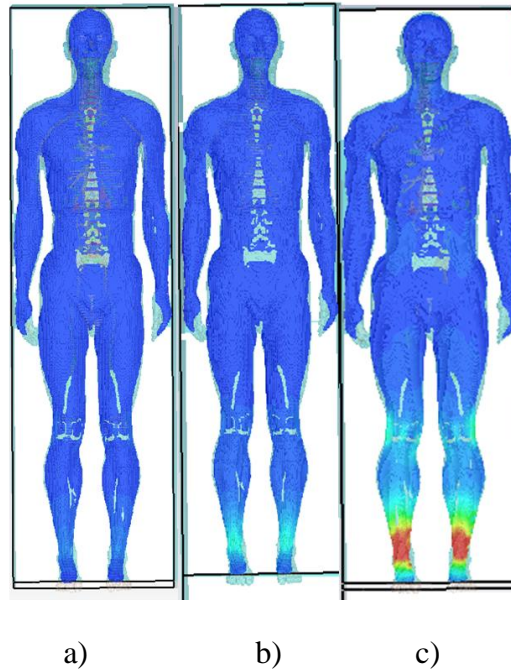
a)　　　　　　b)　　　　　　c)

Fig 3.11 SAR distributions within a human phantom illuminated by a 1W vertically
polarised plane-wave (Ez)
a) wearing shoes standing on PEC boundary b) barefoot standing on 0.5m thick average
ground c) wearing shoes standing on 1m thick perfect electric conduction.

Considering a lossy average ground condition, Fig 3.12 shows the comparison between
calculated WBSAR for Duke and Billie using SEMCAD with various ground brick
thickness models. Fig 3.13 compares computed ankle current in the same scenario. It can
be seen in Fig. 3.12 that shoes reduce whole body SAR; while varying the ground brick
thickness can change the simulated result by approximately $1.5\,\mu$W/kg (20% of the
average calculated value) with Duke standing barefoot on the ground. Billie appears less
affected by the ground brick thickness. Duke and Billie both have higher WBSAR when
the ground brick thickness is between 1.5 and 2 meters which is approximately the height
of the human phantom. Duke's barefoot WBSAR had a pronounced $0.75\,\mu$W/kg (30%)
drop when the ground brick thickness is increased from 2 to 2.5 meters while Billie's
barefoot WBSAR increases by about $0.31\,\mu$W/kg (10%) when the ground brick thickness
is increased from 0.5m to 1.0m. When the human phantom is wearing shoes, the WBSAR
results show less dramatic changes. It also can be seen that when the ground brick
thickness is over 4 meters the WBSAR becomes stable with little variation (about 5%).
The calculated ankle current of both Billie and Duke had the similar trends as shown in

Fig 3.13. When the human is exposed to a uniform field, the induced currents within the body are correlated well with the external electric field strength. The foot current of a grounded person standing in a uniform electric field can be predicted relatively accurately with the equation [3.22].
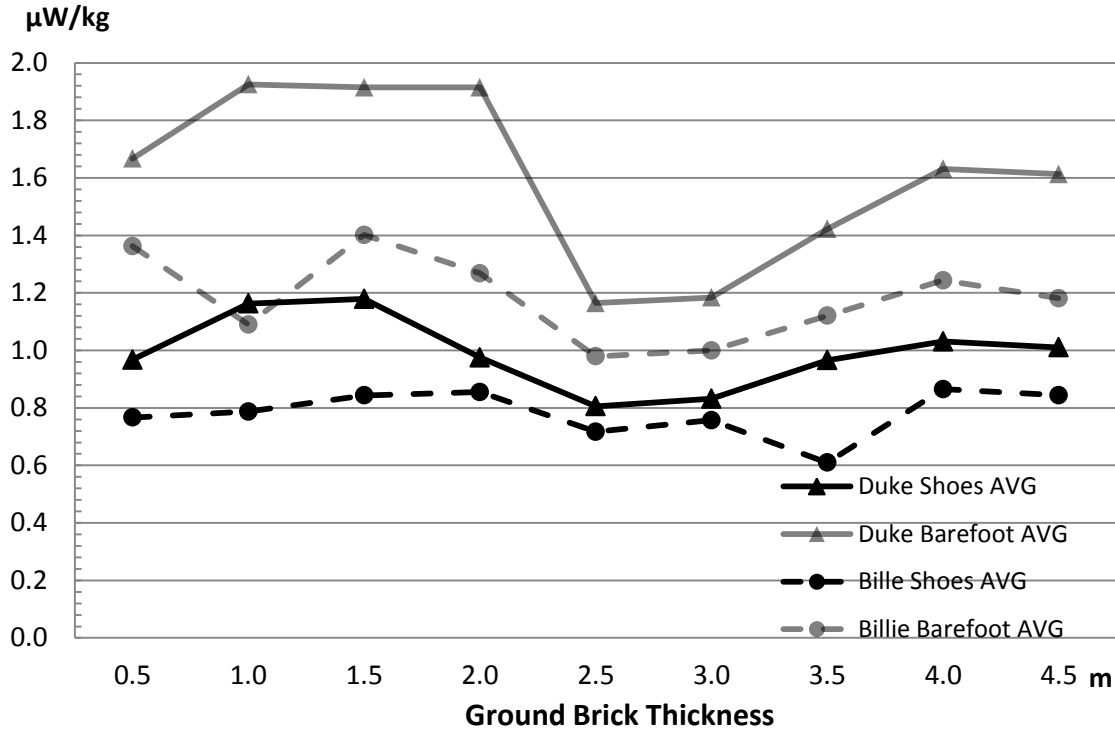
μW/kg

Fig 3.12 Various ground brick thickness WBSAR (μW/kg) comparison in SEMCAD 1V/m vertical polarized plane-wave irradiation.
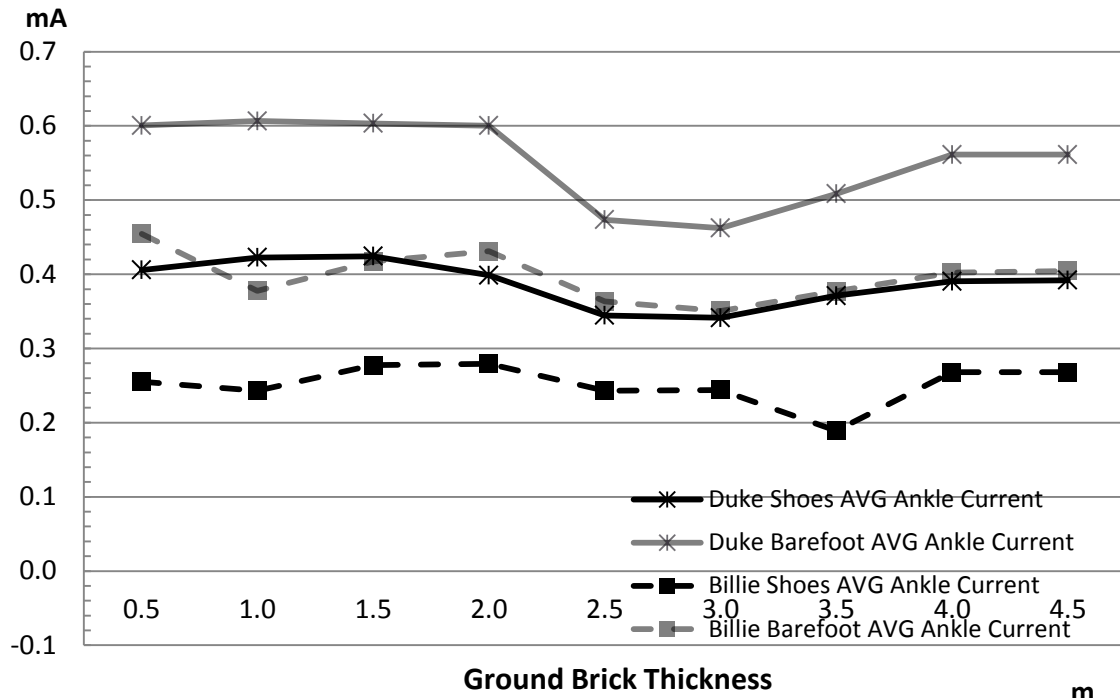
Fig 3.13 Various ground brick thickness ankle current (mA) comparison 1V/m plane-wave irradiation.

Derived electric field levels for comparison with the ICNIRP limits are shown in Table 3.8. The WBSARS in Table 3.13 are based on a phantom with 2mm resolution and 77 tissue types using 1V/m vertically polarized plane-wave illumination.

The ICNIRP Reference Level is compared with the calculated electric field values required to reach the Basic Restrictions on WBSAR. The plots in Table 3.8 and Fig 3.14 present the derived electric field levels required to produce the limits on WBSAR set by ICNIRP for occupational and public exposure. All columns representing these calculations lie within ICNIRP reference levels, therefore the reference levels in these cases provide a conservative estimate of the basic restrictions. The situation in which the strongest coupling conditions exist between the body and the field is barefoot on a ground plane; the situation for Duke is almost twice that for Billie. The WBSAR values for Norman are close to those for Billie modelled above a PEC Boundary (50%). Norman's WBSAR values are almost three times higher than those of both Duke and Billie when they wear shoes and are grounded. Results from ground brick thickness modelling in this chapter

shows that WBSAR falls sharply between 2m and 3m thick. Then rises gradually to the previous level and remains stable as shown in Fig 3.13. It needs to be noted that these models were all located above a 1m brick. For this case the WBSARs are generally in a higher region as shown in Fig 3.12. The results of this section show that 1m thickness brick is sufficient for representing ground conditions.

The derived electric field level required to produce the Basic Restriction on WBSAR compares with the ICNIRP reference levels of 101V/m for occupational exposure and 35V/m for public exposure at 6MHz. When in the grounded situation it was necessary to use higher field strength values in order to produce the same occupational reference level of WBSAR in Duke and Billie. When the field was vertically polarized, the strongest coupling condition, to produce the ICNIRP reference level for Duke, the E-field level required 528V/m barefoot and 599V/m with shoes. Billie required 660V/m barefoot and 713V/m with shoes. In isolated condition Norman, Duke and Billie showed a very good agreement. The highest required E-field values to produce the occupational basic restriction limits are highlighted in red in Table 3.8. The comparison in Table 3.8 clearly shows that when the human phantoms wear shoes isolated over ground - a realistic ground condition (AVG) - Duke requires more than 50% and Billie 8% higher E-field than a PEC ground to generate a WBSAR to exceed the ICNIRP limits. When the human phantoms are barefoot standing on the ground, Duke needs 64% and Billie 53% higher incident field values to exceed the ICNIRP limits. In both cases, Billie needs approximately 20% higher E-field values than Duke to exceed the limits.

Frequency (6MHz)		Norman			Duke			Billie		
		+WBSAR	E-field required for OBRL*	E-field required for PBRL**	+WBSAR	E-field required for OBRL*	E-field required for PBRL**	+WBSAR	E-field required for OBRL*	E-field required for PBRL**
Isolated		0.536	**863.9**	386.3	0.568	**839.2**	375.3	0.575	**834.1**	373.0
Barefoot	PEC Brick				5.166	**278.3**	124.4	2.541	**396.8**	177.4
Barefoot	(++BF)PEC Boundary	4.890	**286.0**	127.9	1.434	**528.1**	236.2	0.918	**660.1**	295.2
Barefoot	(++BF)AVG				1.925	**455.8**	203.9	1.093	**605.0**	270.5
Shoes	PEC Brick				2.529	**397.7**	177.9	0.919	**659.7**	295.0
Shoes	PEC Boundary	2.830	**376.0**	168.1	1.114	**599.2**	268.0	0.948	**649.6**	290.5
Shoes	AVG				1.163	**586.5**	262.3	0.787	**712.9**	318.8

Table 3.8 Calculated Whole-body SAR and calculated electric field values required to produce basic restrictions on whole-body SAR for both occupational and public exposure in SEMCAD.

E-field: V/m
+WBSAR: Whole-body averaged SAR (µW/kg)
++BF: Barefoot
*ICNIRP Occupational basic restriction limit (OBRL) is 0.4W/kg
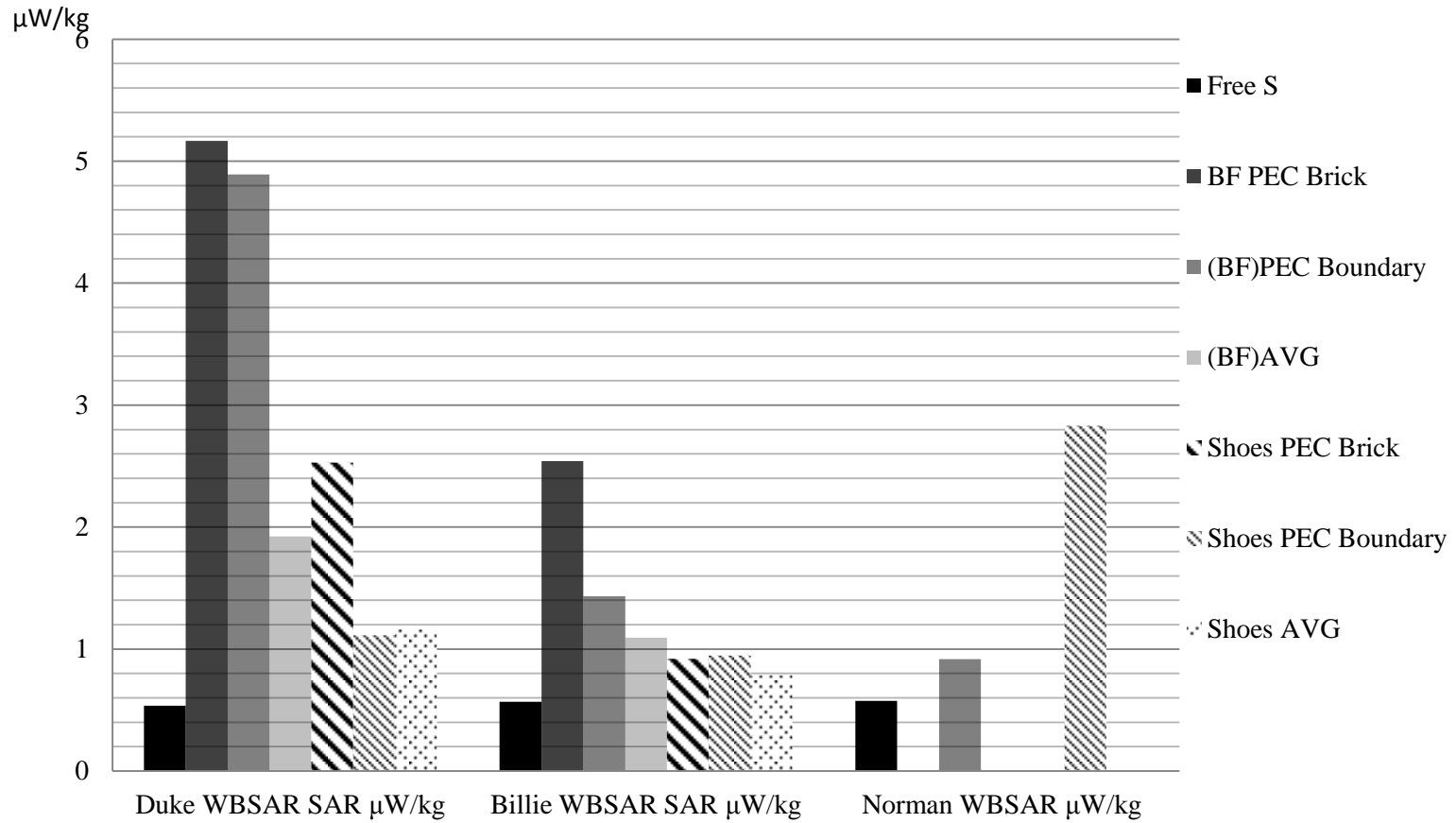**ICNIRP Public basic restriction limit (PBRL) is 0.08W/kg

Fig. 3.14 Calculated whole-body SAR of various human phantom and comparison with Norman.

From Fig. 3.14 it can be seen that the whole-body averaged SAR of Duke and Billie in isolated condition, wearing shoes on a PEC boundary and on wearing shoes on average ground are similar. With the shoe layer included and in the case where Duke and Billie are standing on PEC brick, the WBSAR of Duke is approximately 1.2μW/kg, whilst the WBSAR of Billie is about 0.8μW/kg; about 67% of Duke. Without shoes, in isolation, when barefoot or are standing on a PEC, Duke has the higher WBSAR; almost double the value of Billie on the PEC brick and triple on PEC boundary conditions. When the models are barefoot and standing on average ground the WBSAR for Duke is 70% higher than that of Billie. In P J Dimbylow's [3.1], [3.4], [3.13] work, Norman is over PEC ground, the boundary condition being defined in Fortran programming code based on perfectly matched layers. This is the same as the SEMCAD or CST default boundary condition. The real ground condition was not considered by the HPA or ICNIRP. In the simulated WBSAR results table 3.8 and Fig. 3.14 Norman has a good agreement with Duke and Billie are isolated, but is almost three times higher than Duke and Billie when barefoot or wearing shoes and grounded. The value for Duke is about four times higher than Norman, and that for Billie is just over double when barefoot and grounded. In the isolated condition the simulated WBSAR results for Norman appear to be approximately three times higher than for Duke and Billie; the result for Duke is only 0.2μW/kg higher than that for Billie.

3.6 Conclusions

This chapter studied the external electric field values corresponding to restrictions on whole body SAR. In the preliminary modelling and analysis stage the homogenous phantom for SAR calculation is inadequate. However, it showed different current density distributions in the human torso and leg when the polarization of the dominant electrical field is horizontal or vertical. Therefore high resolution heterogeneous voxel phantoms - Duke and Billie from the Virtual Family - were considered. The effects of differences in ground plane modelling and shoe thickness are also studied in this chapter. It has been shown that the modelling parameters have a significant influence on the results of calculations. The calculation of averaged whole-body SAR and the derived electric field compared with ICNIRP Basic Restriction limits demonstrate that, in order to produce the

whole-body SAR restriction level at the given frequency, much higher electric field strengths than those given in the ICNIRP guidelines were required for both public and occupational exposure. The EMF analysis in the near-field region of a high power HF broadcast transmitting antenna is crucial and will be discussed in the following chapter. The characterisations of several modelling parameters shown in this chapter are useful in establishing a methodology for human radiation hazard assessment at various HF broadcasting transmitter sites.

The Virtual Family has a good level of agreement with Norman in various simulations, using both CST microwave studio and SEMCAD. The Virtual Family of commercially available anatomical human phantoms has provided credible results to be used in further studies.

The FDTD-MoM hybrid method was employed in the study has shown itself to be a very efficient way to reduce the computational hardware and resource requirements needed to calculate SAR directly. However, because SEMCAD is capable of simulating a full scale transmitting curtain antenna further investigation should be considered. This constraint of the Huygen Box for this is that it requires a third software package to import the EMF from the region of interest in front of the array. This requires further investigation and validation.

The effect of the layer thickness (of the soles) of shoes on the WBSAR calculation indicates that, in a realistic human exposure situation, the WBSAR value would be lower than other researchers have shown. However, for a conservative evaluation point of view, flat (bottomed) feet or various thicknesses of shoes could have impact on the calculated WBSAR. This study also considered the phantom being barefoot or wearing shoes over PEC and average lossy grounds. The earlier UK HPA study only considered the human being barefoot or wearing shoes over a PEC. When comparing the WBSAR of Duke with Norman either barefoot or with shoes, the results vary depending on the ground condition applied. The results in this study show that the ground condition has a significant effect on the energy absorption in the human body. By using a brick to represent ground, the results have shown this modelling technique could be applied to further research or similar EM

exposure problems. The results of this chapter show that 1m thickness brick is sufficient for representing ground condition modelling.

References

[3.1] P. Dimbylow, "Assessing the compliance of emissions from HF broadcast transmitters - with exposure guidelines," 2006.

[3.2] P. Dimbylow, "SAR in the mother and foetus for RF plane wave irradiation.," *Physics in medicine and biology*, vol. 52, no. 13, pp. 3791–802, Jul. 2007.

[3.3] A. Hirata, O. Fujiwara, T. Nagaoka, and S. Watanabe, "Estimation of Whole-Body Average SAR in Human Models Due to Plane-Wave Exposure at Resonance Frequency," *IEEE Transactions on Electromagnetic Compatibility*, vol. 52, no. 1, pp. 41–48, Feb. 2010.

[3.4] P. Dimbylow, "Assessing the compliance of emissions from MF broadcast transmitters - including exposure guidelines," 2006.

[3.5] International Commission on Non-Ionizing Radiation Protection, "Guidelines for limiting exposure to time-varying electric, magnetic, and electromagnetic fields (up to 300 GHz)," *Health Phys.*, vol. 74, no. 4, p. 494, 1998.

[3.6] R. Guide, "SEMCAD X Reference Guide," *The International Executive*, vol. 30, no. 2. pp. 35–99, 1988.

[3.7] Y. F. Y. Fu, G. Cook, M. Hate, D. Fisher, and J. McCalla, "EMC compliance testing of BBC World Service HF transmitter sites," in *Antennas & Propagation ...*, 2009.

[3.8] K. . Yee, "Numerical solution of initial boundary value problems involving Maxwell's equations in isotropic media," *IEEE Trans. Antennas Propag.*, vol. 14, no. 3, p. 302, 1966.

[3.9] J. Berenger, "A perfectly matched layer for the absorption of electromagnetic waves," *J. Comput. Phys.*, vol. 114, no. 2, p. 185, 1994.

[3.10] R. P. Findlay, P. J. Dimbylow, H. Search, C. Journals, A. Contact, M. Iopscience, and I. P. Address, "Variations in calculated SAR with distance to the perfectly matched layer boundary for a human voxel model.," *Physics in medicine and biology*, vol. 51, no. 23, pp. N411–5, Dec. 2006.

[3.11] P. J. Dimbylow, "FDTD calculations of the whole-body averaged SAR in an anatomically realistic voxel model of the human body from 1 MHz to 1 GHz.," *Physics in medicine and biology*, vol. 42, no. 3, pp. 479–90, Mar. 1997.

[3.12] D. Merewether, "On implementing a numeric Huygen's source scheme in a finite difference program to illuminate scattering bodies," *… , IEEE Transactions on*, no. 6, pp. 1829–1833, 1980.

[3.13] P. J. Dimbylow, "Fine resolution calculations of SAR in the human body for frequencies up to 3 GHz.," *Physics in medicine and biology*, vol. 47, no. 16, pp. 2835–46, Aug. 2002.

[3.14] R. Harrington, *Field computation by moment methods*. 1993.

[3.15] A. Taflove, "Application of the Finite-Difference Time-Domain Method to Sinusoidal Steady-State Electromagnetic-Penetration Problems," *Ieee Transactions On Electromagnetic Compatibility*, vol. EMC-22, no. 3, pp. 191–202, 1980.

[3.16] "Numerical Electromagnetics Code NEC-4." University of California, Livermore, Ca 94551, Technical Information Dept., Lawrence Livermore National Laboratory.

[3.17] SPEAG, "SEMCAD X®." Schmid &Partner Engineering AG http://www.speag.com/.

[3.18] Y. Fu, M. Hate, J. McCalla, R. Langle, and J. Rigelsford, "Assessment of Equivalence Principles Method for HF near-field exposure modelling," in *2011 Loughborough Antennas Propagation Conference*, 2011, pp. 1–4.

[3.19] P. J. Dimbylow, "The calculation of induced currents and absorbed power in a realistic, heterogeneous model of the lower leg for applied electric fields from 60 Hz to 30 MHz.," *Physics in medicine and biology*, vol. 33, no. 12, pp. 1453–68, Dec. 1988.

[3.20] P. J. Dimbylow, "Induced current densities from low-frequency magnetic fields in a 2 mm resolution, anatomically realistic model of the body.," *Physics in medicine and biology*, vol. 43, no. 2, pp. 221–30, Feb. 1998.

[3.21] D. W. Deno, "Currents induced in the human body by high voltage transmission line electric field-Measurement and calculation of distribution and dose," *IEEE Transactions on Power Apparatus and Systems*, vol. 96, no. 5, pp. 1517–1527, Sep. 1977.

[3.22] K. Jokela and L. Puranen, "Occupational RF exposures," *Radiation protection dosimetry*, vol. 83, no. 1999, pp. 119–124, 1999.